Global trends in carbon sinks and their relationships with CO_2 and temperature

Authors: M. Fernández-Martínez*[1]. J. Sardans[2,3], F. Chevallier[4], P. Ciais[4], M. Obersteiner[5], S. Vicca[1], J. G. Canadell[6], A. Bastos[4], P. Friedlingstein[7], S. Sitch[7], S.L. Piao[8,9], I.A. Janssens[1], J. Peñuelas[2,3].

Affiliations:

[1] Centre of Excellence PLECO (Plant and Vegetation Ecology), Department of Biology, University of Antwerp, 2610 Wilrijk, Belgium.

[2] CSIC, Global Ecology Unit, CREAF-CSIC-UAB, Cerdanyola del Vallès, 08193 Barcelona, Catalonia, Spain

[3] CREAF, Cerdanyola del Vallès, 08193 Barcelona, Catalonia, Spain

[4] Laboratoire des Sciences du Climat et de l'Environnement, CEA CNRS UVSQ, 91191 Gif-sur-Yvette, France

[5] International Institute for Applied Systems Analysis, Schlossplatz 1, 2361 Laxenburg, Austria

[6] Global Carbon Project, CSIRO Oceans and Atmosphere, Canberra, ACT 2601, Australia

[7] College of Engineering, Computing and Mathematics, University of Exeter, Exeter EX4 4QF, UK

[8] Sino-French Institute of Earth System Sciences, College of Urban and Environmental Sciences, Peking University, Beijing 100871, China

[9] Institute of Tibetan Plateau Research, Chinese Academy of Sciences, Beijing 100085, China

*Correspondence to: M. Fernández-Martínez, marcos.fernandez-martinez@uantwerpen.be

Length of the main text: 3415 words
Length of the methods: 1490 words
Figures and tables: 2 figures, 2 tables
Length of the captions: 512 words
References: 49

Abstract

Elevated CO_2 increases photosynthesis and, potentially, net CO_2 uptake by ecosystems (NEP). Climate, nutrients, and ecosystem structure, however, influence the effect of increasing CO_2. Here, we analysed global NEP from MACC-II and Jena CarboScope atmospheric-inversions and 10 dynamic global vegetation models (TRENDY), using statistical models to attribute the trends in NEP to its potential drivers: CO_2, climatic variables and land-use change. Increasing CO_2 was consistently associated with increased NEP from 1995 to 2014. Conversely, increasing temperatures were negatively associated with NEP. Using the two atmospheric inversions and TRENDY, the estimated global sensitivities for CO_2 were 6.0 ± 0.1, 8.1 ± 0.3 and 3.1 ± 0.1 Pg C per 100 ppm (~1 ºC increase), and -0.5 ± 0.2, -0.9 ± 0.4 and -1.1 ± 0.1 Pg C $°C^{-1}$ for temperature. Our results indicate a positive CO_2 effect on terrestrial C sinks and that climate warming is constraining it.

Main text

In recent decades, terrestrial ecosystems have been absorbing 15–30% of all anthropogenic CO_2 emissions[1,2]. Direct and indirect anthropogenic impacts on the biosphere, however, can alter terrestrial sinks in the short and long terms[3–6]. Identifying the factors that affect the capacity of the biosphere to absorb carbon (C) and quantifying the magnitude of the sensitivity of this C sink to its driving factors helps to increase confidence in future projections of the coupled C cycle/climate system.

Increasing plant growth is a robust response to increasing CO_2 concentrations under experimental conditions (CO_2 fertilization effect)[7,8]. The scientific community, however, is still trying to determine to what extent the increase in CO_2 can enhance large-scale photosynthesis and ultimately net ecosystem production (NEP)[5,7]. Detecting the effect of elevated CO_2 on C fluxes in the real world is much more difficult than under controlled experiments. However, recent efforts using eddy-covariance-based data and statistical models have been successful in detecting positive effects of CO_2 on water-use efficiency (WUE)[9], photosynthesis, and NEP[5].

The potential positive effect of elevated CO_2 on productivity could be influenced by global warming[6] and altered precipitation patterns[10] since both water availability and temperature are strong drivers of photosynthesis and respiration worldwide[11–13]. Land-use change also alters the capacity of the biosphere to sequester C because land use causes a drastic change in C turnover and productivity. Atmospheric deposition of nitrogen (N) and sulphur (S) from the use of fossil fuels and fertilisers may also alter ecosystem biodiversity, function, productivity and NEP[5,14–17]. N deposition is usually positively correlated with ecosystem productivity and NEP[17–19]. Conversely, S deposition may reduce ecosystem carbon sinks, but it is poorly studied in field studies[20,21] and absent from global models. Soil acidification, caused by acid deposition, of N and S, often decreases the availability of soil nutrients[22] and potentially reduces NEP[23].

The observations underlying the driver analysis of NEP described above were largely limited to temperate and boreal study sites, making it difficult to assess whether or not these results are scalable globally. Additionally, until recently, the only way to assess terrestrial C sink has been from ensembles of dynamic global vegetation models (DGVMs) or as a residual sink, by subtracting atmospheric and ocean sinks to the estimates of CO_2 emissions. Currently, inversion models, as well as long-term remotely sensed data[24], can be used to test the generality of the patterns derived from ground-based measurements. Inversion models provide continuous gridded estimates for the net flux of land-atmosphere CO_2 exchange (i.e. NEP) with global coverage[25,26]. The gridded NEP results from inversions, combined with CO_2-concentration records, gridded fields for climate, land-use change, and atmospheric deposition, are arguably the best observation-based data to attempt a first empirical study of the combined effects of CO_2, changes in climate and land use, and atmospheric N and S deposition on terrestrial NEP patterns at the global scale. Given that previous studies at the site level revealed that increasing CO_2 is a dominant driver of trends in NEP, we here expect that it will also be the dominant driver at larger spatial scales and across the globe.

Hence, we here investigate if the trends of NEP from the two most widely used multi-decadal inversion models (MACC-II and Jena CarboScope) and DGVMs (TRENDY) from 1995 to 2014 are related to increasing atmospheric CO_2 and changing climate (temperature, precipitation, and drought). We also investigated the effect of land-use on NEP at the global scale. To do so, we used statistical models to assess the sensitivity of NEP to the abovementioned predictors. We also analysed the effect of changing rates of atmospheric deposition of oxidised and reduced N and S on NEP, combined with increasing CO_2 and changing climate and land use, over Europe and the United States of America (USA).

Global trends in NEP, and the contributions of CO_2 and climate

Global land (except the Antarctica) mean annual NEP was 2.3 ± 0.9, 2.3 ± 1.5 and 1.6 ± 0.5 Pg y^{-1} (mean ± 1σ), respectively, for MACC-II, Jena CarboScope and the TRENDY ensemble during the period 1995–2014, similar in magnitude to recent reports of the global carbon budget[2]. Both inversions and the TRENDY ensemble showed an overall positive trend in NEP from 1995 to 2014. The estimated NEP increased by (mean ± 1SE) 116.9 ± 6.1 Tg C y^{-1} for the MACC-II dataset, by 178.0 ± 8.1 Tg C y^{-1} for the Jena CarboScope dataset, and by 22.5 ± 3.1 Tg C y^{-1} for the TRENDY ensemble (**Figure 1**). This result also agrees with the increases reported in the last global carbon budget[2], showing a lower increase of the DGVMs than those shown by the inversion models. The large differences between inversion models and DGVMs may arise because of the lack of information on river fluxes, inadequate parameterisations concerning land management and degradation in the process models or because of potential biases in inversion models. Both MACC-II and Jena CarboScope datasets produced similar trends for many parts of the world, an increasing NEP for Siberia, Asia, Oceania, and South America, and a decreasing NEP for the southern latitudes of Africa. Differences between inversions emerged for Europe and North America, possibly because Jena CarboScope inversion uses a larger spatial error correlation of prior fluxes than MACC-II or because of other inversion settings[2]. However, their different flux priors did not drive differences in the trends between both datasets, given that priors did not change over the studied period. Jena CarboScope showed largely positive trends for Europe and largely negative trends for North America; MACC II showed more variation in the trends for both continents. The trends identified by the TRENDY ensemble agreed with atmospheric inversions for the northernmost latitudes, indicating an increase in C-sink capacity, but differed from those in many other regions. Again, these differences may indicate inadequate parameterisation of the DGVMs or biases on the inversion models.

Our analyses on temporal contributions, using the temporal anomalies of our predictors, attributed the increases in global NEP to increasing CO_2 but found a consistent negative impact of temperature on NEP, which limited the positive effect of increasing CO_2 (**Figure 1**). These results were consistent for both datasets and most of the DGVMs of the TRENDY ensemble. The predictors used in this study explained a modest proportion of the variance in NEP, in contrast to the variance explained by spatial variability (i.e., the pixel), which was rather high (**Supplementary Information, 2**). Unknown contributions to trends in NEP, the difference between all contributions and the observed trend, were very close to zero for the analyses on inverse models and the TRENDY ensemble (**Figure 1**). This result suggests that trends were very well captured by our analyses, indicating that our methodology was able to disentangle spatial from temporal variability. The sensitivity of NEP to increasing CO_2 averaged 0.45 ± 0.01, 0.61 ± 0.03 and 0.23 ± 0.01 g C m^{-2} ppm^{-1} for MACC-II, Jena CarboScope and TRENDY, respectively **(Table 1)**, representing sensitivities over the entire terrestrial surface of 60.4 ± 1.2, 81.4 ± 3.4 and 30.7 ± 1.2 Tg C ppm^{-1}, respectively. Despite lower temporal attributions for temperature than CO_2, the sensitivity of NEP to temperature was high, at -3.8 ± 1.1, -6.4 ± 2.9 and -8.1 ± 0.9 g C m^{-2} y^{-1} $°C^{-1}$ for the MACC-II, Jena CarboScope and TRENDY models, respectively, equivalent to global sensitivities of -515.7 ± 152.4, -859.2 ± 386.3 and -1088.0 ± 118.1 Tg C $°C^{-1}$, respectively. Despite trends in NEP and the effect of CO_2 and temperature on NEP significantly differed in magnitude amongst the datasets used, they all point towards the same conclusion: global NEP has increased during the study period and increasing CO_2 has been the most likely factor driving this increase despite increasing temperatures are constraining this positive effect. The exact magnitude of the effect of increasing CO_2 and temperatures on global carbon cycle remains, thus, still under debate.

Spatial variability on CO_2 and climate change effects on NEP

Our statistical models for the MACC-II and Jena CarboScope datasets indicated that the positive effect of CO_2 on NEP was higher in regions with higher annual precipitation and that this positive effect increased with increasing temperatures (**Figure 2, Supplementary Information 1.1**). Instead, our analyses using the TRENDY ensemble did not show a significant interaction between CO_2 and precipitation and neither with temperature, highlighting again the different behaviour showed by the DGVMs compared to inversion models. We also found a positive significant interaction between mean annual temperature and CO_2 for Jena CarboScope and TRENDY. However, the same interaction was negative for MACC-II. On the other hand, increasing temperatures reduced NEP in warm regions but increased NEP in cold regions (**Figure 2**).

The analyses on temporal contributions performed for inversion and TRENDY NEP averaged over latitudinal bands (boreal, >55°; temperate, 35-55°; subtropical, 15-35°; and tropical, 15°N-15°S), further supported the previous results obtained at the global scale (**Table 2, Supplementary Information 2.2–2.7**). Increasing CO_2 was the main factor accounting for increasing trends in NEP, with a consistent positive temporal contribution for almost all latitudinal bands considered and for all three datasets. However, contributions estimated from the TRENDY ensemble were generally lower than those of the inversion models. Proportionally, increasing CO_2 accounted for more than 90% of the trends in NEP in MACC-II and Jena CarboScope datasets. For the TRENDY ensemble, the estimated contribution of CO_2 to the trends in global NEP was more than 2.7 times higher than the estimated trends. Increasing temperatures had a negative effect for all latitudinal bands for the inversion models, but most effects were not statistically significant and need to be interpreted as such. Instead, our analyses for the TRENDY ensemble indicated a significant negative effect for all latitudinal bands, except for the temperate southern hemisphere. Similarly, the proportional contribution of temperature to the trends in NEP was less than 10% for the inversion models, but accounted for almost 95% of the trends estimated using the TRENDY ensemble. These results suggest that the parameterisation of temperature in the DGVMs does not accurately reproduce the estimation of the inverse models.

Despite all regions presented, on average, positive trends, the tropical regions were clearly those with the highest contribution to global NEP trends using all three datasets, accounting for almost half of the global NEP increase (**Table 2**). Similarly, the tropical regions were those with the highest sensitivity to CO_2 increase, accounting for more than half of the total global sensitivity (**Table 1**). A similar pattern was found for temperature, despite the sign of the contribution was positive for MACC-II but negative for Jena CarboScope and TRENDY. The contribution of the southern hemisphere to the global trends in NEP was very modest compare to the contribution of the northern hemisphere using all datasets. Our results using the MACC-II dataset showed that subtropical, temperate and boreal regions accounted for 44.2% of the global trends in NEP, while only 9.5% was attributed to subtropical and temperate regions of the southern hemisphere. Using the Jena CarboScope dataset we found that 63.3% of the global trends were attributed to subtropical, temperate and boreal regions of the northern hemisphere, while only 6.1% was attributed to subtropical and temperate zones of the southern hemisphere. Differences on the regional attributions between inversion models may emerge from the different interhemispheric transport models or other inversion settings[2]. Results from the TRENDY ensemble were more extreme, because they indicated a negative contribution of the subtropical and temperate regions to the global trends in NEP. Differences between the global estimates (trends and contributions of CO_2 and temperature) and the sum of every region were low for all datasets. Contribution of other variables to the trends in NEP (precipitation, drought, land-use change, and unknown variables) were on average also low for most of the latitudinal bands, despite the variability amongst datasets (**Table 2**).

Analyses of atmospheric deposition over Europe and the USA

The MACC-II and Jena CarboScope datasets showed that NEP increased over Europe and the USA by 0.45 ± 0.13 and 0.68 ± 0.16 g C m^{-2} y^{-1}, respectively (**Figure S1**). Our temporal contribution analyses suggested that increasing atmospheric CO_2 in both datasets contributed significantly to increasing NEP. NEP sensitivity to CO_2 was more than two-fold higher in the Jena CarboScope than the MACC-II dataset (**Table S1**), similar to the temporal contributions, at 0.22 ± 0.06 and 0.46 ± 0.07 g C m^{-2} y^{-1} ppm^{-1} for the MACC-II and Jena CarboScope models, respectively. The temporal contribution of decreasing N_{OX} deposition to NEP differed between the two datasets; the contribution was positive for MACC-II and negative for Jena CarboScope. Our analyses consequently estimated a negative sensitivity of NEP to N_{OX} for the MACC-II dataset but a positive sensitivity for the Jena CarboScope dataset. Additionally, neither MACC-II, nor Jena CarboScope indicated a strong impact of land use change.

Our statistical models indicated that, in both datasets, the positive effect of CO_2 on NEP was higher in regions with higher N_{RED} deposition but lower in regions with high S deposition (means for MACC-II and annual anomalies for Jena CarboScope; see

Supplementary Information 2.8). The results for N_{OX} deposition, however, differed between the models. The positive effect of CO_2 on NEP for the MACC-II dataset was constrained by the annual anomalies of N_{OX} but was higher for the Jena CarboScope dataset. We also estimated an overall negative but not significant sensitivity of NEP to S deposition for both inversion models.

Effect of CO_2 fertilisation on global NEP

NEP is the net result of multiple processes that consume or produce CO_2 (i.e. photosynthesis, autotrophic respiration [Ra], and heterotrophic respiration [Rh]). The positive effect of atmospheric CO_2 on NEP must therefore originate from a stronger positive effect on photosynthesis than on the sum of all respiratory processes. Increasing atmospheric CO_2 concentrations have been widely reported to increase ecosystem photosynthesis, mainly by two mechanisms: i) increasing carboxylation rates and decreasing photorespiration[27], and ii) decreasing stomatal conductance and therefore increasing WUE[9,28], which would theoretically increase photosynthesis under water limitation. An increase in GPP by either mechanism may thus account for the higher NEP due to increasing atmospheric CO_2. A recent global analysis suggested that most of the GPP gains from CO_2 fertilization are associated with ecosystem WUE[29]. The positive interaction between CO_2 and annual precipitation that we found may not support this hypothesis (**Figure 2**), given that plants living under wet conditions are usually less efficient in the use of water. However, plants having higher water availability may be able to benefit from increasing CO_2 more than those suffering drought because photosynthesis would not be water-limited.

Our estimates of global NEP sensitivity to CO_2 were 0.45 ± 0.01, 0.61 ± 0.03 and 0.23 ± 0.01 g C m^{-2} ppm^{-1} (globally 60.4 ± 1.2, 81.4 ± 3.4 and 30.7 ± 3.4 Tg C ppm^{-1}) for the MACC-II, Jena CarboScope and TRENDY datasets, respectively, but these estimates varied amongst the latitudinal bands and were inconsistent between datasets (**Table 1**). These estimates were similar to those reported in CO_2-enrichment FACE experiments[30], despite the fact that FACE values were calculated for a much higher CO_2 range for which the effect of CO_2 may saturate[31]. However, they were much lower than the 4.81 ± 0.52 g C m^{-2} ppm^{-1} reported in a study using eddy-covariance flux towers for a similar period[5]. The much larger areas analysed by the inverse models than the footprints covered by the eddy-covariance flux towers, and FACE experiments, may explain these differences between the estimates. Flux towers are usually located in relatively homogenous, undisturbed ecosystems, while each pixel in the inverse model aggregates information from several ecosystems (and even biomes), often including non-productive land such as bare soil or cities.

Our results indicated that the variability of the estimates of NEP sensitivity to CO_2 amongst the latitudinal bands might be associated with differences in climate and atmospheric N and S deposition. The two atmospheric inversion models indicated that the effect of CO_2 fertilisation was stronger in wet climates (high annual precipitation) (**Figure 2**), supporting the estimates provided by the latitudinal bands, with the highest sensitivity estimates for the tropical band (**Table 1**). However, analyses based on the TRENDY ensemble did not show the same results. The positive effect of CO_2 tended to increase with temperature anomalies in both inversion models, but, again, the DGVMs did not show the same behaviour. These differences between inversion models and process-based models suggest that DGVMs still fail to capture some of the interactions occurring in nature. The MACC-II and Jena CarboScope datasets further agreed on a stronger positive effect of increasing CO_2 in regions with higher N_{RED} deposition, which confirms previous studies suggesting that the effect of CO_2 fertilisation is stronger in nitrogen-rich sites[32–34].

Climate, land-use changes and C sinks

Climatic warming clearly had a secondary effect on the trends in NEP from 1995 to 2014. The MACC-II, Jena CarboScope and TRENDY datasets estimated that NEP decreased globally by around -0.5 ± 0.2, -0.9 ± 0.4 and -1.1 ± 0.1 Pg C for every degree of increase in the Earth's temperature. Assuming that a CO_2 increase of 100 ppm is equivalent to an increase of global temperature of 1 ºC, the effect of the increasing CO_2 concentrations largely outweighs the negative effect of increasing temperature on NEP (global estimates: 6.0 ± 0.1, 8.1 ± 0.3 and 3.1 ± 0.1 Pg C for a 100 ppm of CO_2 increase according to MACC-II, Jena CarboScope and TRENDY). The difference, though, is much lower for TRENDY than for the inversion models, having a higher negative impact of temperature and a lower positive effect of CO_2. This difference in the effects of temperature and CO_2 may explain the lower trends observed in TRENDY datasets compared to MACC-II and Jena CarboScope. It also suggests that a different parameterisation of temperature, CO_2 and their interaction may be needed on DGVMs to capture the observed trends on the inversion models.

The quasi monotonically increasing atmospheric CO_2 concentrations have thus been more important than temperature in driving NEP trends. Increasing temperature, however, did not have the same effect on NEP around the world. The analyses for both inverse models indicated that increasing temperatures had a positive effect on NEP only in cold regions (when MAT ≤ 1.5, 9 and -5.9 ºC for MACC-II and Jena CarboScope and TRENDY respectively, when CO_2 = 400 ppm, see **Supplementary Information 2.1**, and **Figure 2**). These findings support previous literature reporting a positive effect between temperature increase and NEP in temperate and boreal forests[35]. Instead, the general negative effect of temperature on NEP could be due to a greater stimulation of Re than photosynthesis by higher temperatures[36,37]. The potential benefit to C sequestration of increased photosynthesis would then be negated by a higher increase in Re. Increasing temperatures can also be linked to heat waves and drier conditions, which may decrease GPP more than Re[38].

The effects of land-use change on the NEP trends differed greatly amongst the datasets, both at the global scale and when using latitudinal bands. Our statistical models identified several statistically significant relationships between NEP and land-use change, but the large differences in effects (direction and magnitude) amongst the datasets preclude drawing firm conclusions. Likely, the coarse resolution of our analysis blurred the effects of land-use change on the NEP trends.

Overall, our study highlights the main role of rising atmospheric CO_2 concentrations triggering an increase in land C sinks over the entire planet from 1995 to 2014, while the tropics have accounted for around half of this increase in NEP despite accounting only for around 22% of the global land (excluding the Antarctica, **Table 2**). Therefore, preserving tropical ecosystems should be a global priority in order to mitigate anthropogenic CO_2 emissions. Temperature, instead, has diminished the capacity of terrestrial ecosystems to sequester C, which jeopardises future C sink capacity in light of global warming. So far, our results suggest that the benefit of increasing atmospheric concentrations of CO_2 are still compensating the negative ones because of temperature rise, in terms of C sequestration. However, if it has not started to change already[6], this pattern may reverse soon because of a saturation of land C sinks[5,31] or because as temperature rises warm ecosystems tend to decrease NEP (**Figure 2**). Additionally, the comparison between results of inversion models and the TRENDY ensemble indicated that the DGVMs were unable to reproduce several features of the global land C sinks observed in inversion models. Process-based earth system models will need to improve their parameterisation to capture these features in order to better predict the future of land C sinks.

References:

1. Canadell, J. G. *et al.* Contributions to accelerating atmospheric CO2 growth from economic activity, carbon intensity, and efficiency of natural sinks. *Proc. Natl. Acad. Sci. U. S. A.* **104,** 18866–70 (2007).

2. Le Quéré, C. *et al.* Global Carbon Budget 2017. *Earth Syst. Sci. Data* **10,** 405–448 (2018).

3. Ciais, P. *et al.* Europe-wide reduction in primary productivity caused by the heat and drought in 2003. *Nature* **437,** 529–533 (2005).

4. Crowther, T. W. *et al.* Quantifying global soil carbon losses in response to warming. *Nature* **540,** 104–108 (2016).

5. Fernández-Martínez, M. *et al.* Atmospheric deposition, CO2, and change in the land carbon sink. *Sci. Rep.* **7:9632,** 1–13 (2017).

6. Peñuelas, J. *et al.* Shifting from a fertilization-dominated to a warming dominated period. *Nat. Ecol. Evol.* **1,** 1438–1445 (2017).

7. Ainsworth, E. A. & Long, S. P. What have we learned from 15 years of free-air CO2 enrichment (FACE)? A meta-analytic review of the responses of photosynthesis, canopy properties and plant production to rising CO2. *New Phytol.* **165,** 351–71 (2005).

8. Medlyn, B. E. *et al.* Using ecosystem experiments to improve vegetation models. *Nat. Clim. Chang.* **5,** 528–534 (2015).

9. Keenan, T. F. *et al.* Increase in forest water-use efficiency as atmospheric carbon dioxide concentrations rise. *Nature* **499,** 324–327 (2013).

10. Alexander, L. *et al. Climate Change 2013: The Physical Science Basis - Summary for Policymakers*. *Fifth Assessment Report* (Intergovernmental Panel on Climate Change, 2013).

11. Fernández-Martínez, M. *et al.* Spatial variability and controls over biomass stocks, carbon fluxes and resource-use efficiencies in forest ecosystems. *Trees, Struct. Funct.* **28,** 597–611 (2014).

12. Beer, C. *et al.* Terrestrial gross carbon dioxide uptake: global distribution and covariation with climate. *Science (80-.).* **329,** 834–8 (2010).

13. Luyssaert, S. *et al.* CO 2 balance of boreal, temperate, and tropical forests derived from a global database. *Glob. Chang. Biol.* **13,** 2509–2537 (2007).

14. de Vries, W. & Posch, M. Modelling the impact of nitrogen deposition, climate change and nutrient limitations on tree carbon sequestration in Europe for the period 1900–2050. *Environ. Pollut.* **159,** 2289–2299 (2011).

15. Wamelink, G. W. W. *et al.* Modelling impacts of changes in carbon dioxide concentration, climate and nitrogen deposition on carbon sequestration by European forests and forest soils. *For. Ecol. Manage.* **258,** 1794–1805 (2009).

16. Wamelink, G. W. W. *et al.* Effect of nitrogen deposition reduction on biodiversity and carbon sequestration. *For. Ecol. Manage.* **258,** 1774–1779 (2009).

17. de Vries, W., Du, E. & Butterbach-Bahl, K. Short and long-term impacts of nitrogen deposition on carbon sequestration by forest ecosystems. *Curr. Opin. Environ. Sustain.* **9–10,** 90–104 (2014).

18. Luyssaert, S. *et al.* The European carbon balance. Part 3: forests. *Glob. Chang. Biol.* **16,** 1429–1450 (2010).

19. Magnani, F. *et al.* The human footprint in the carbon cycle of temperate and boreal forests. *Nature* **447,** 848–50 (2007).

20. Thomas, R. B., Spal, S. E., Smith, K. R. & Nippert, J. B. Evidence of recovery of Juniperus virginiana trees from sulfur pollution after the Clean Air Act. *Proc. Natl. Acad. Sci. U. S. A.* **110,** 15319–24 (2013).

21. Oulehle, F. *et al.* Major changes in forest carbon and nitrogen cycling caused by declining sulphur deposition. *Glob. Chang. Biol.* **17,** 3115–3129 (2011).

22. Truog, E. Soil Reaction Influence on Availability of Plant Nutrients1. *Soil Sci. Soc. Am. J.* **11,** 305 (1946).

23. Fernández-Martínez, M. *et al.* Nutrient availability as the key regulator of global forest carbon balance. *Nat. Clim. Chang.* **4,** 471–476 (2014).

24. Zhu, Z. *et al.* Greening of the Earth and its drivers. *Nat. Clim. Chang.* **6,** 791–795 (2016).

25. Chevallier, F. *et al.* CO 2 surface fluxes at grid point scale estimated from a global 21 year reanalysis of atmospheric measurements. *J. Geophys. Res.* **115,**

D21307 (2010).

26. Rödenbeck, C., Houweling, S., Gloor, M. & Heimann, M. CO_2 flux history 1982–2001 inferred from atmospheric data using a global inversion of atmospheric transport. *Atmos. Chem. Phys.* **3,** 1919–1964 (2003).

27. Aber, J. *et al.* Forest Processes and Global Environmental Change: Predicting the Effects of Individual and Multiple Stressors. *Bioscience* **51,** 735 (2001).

28. Prentice, I. C., Heimann, M. & Sitch, S. The carbon balance of the terrestrial biosphere: Ecosystem models and Atmospheric observations. *Ecol. Appl.* **10,** 1553–1573 (2000).

29. Cheng, L. *et al.* Recent increases in terrestrial carbon uptake at little cost to the water cycle. *Nat. Commun.* **8,** 110 (2017).

30. Norby, R. J., Warren, J. M., Iversen, C. M., Medlyn, B. E. & McMurtrie, R. E. CO2 enhancement of forest productivity constrained by limited nitrogen availability. *Proc. Natl. Acad. Sci. U. S. A.* **107,** 19368–73 (2010).

31. Norby, R. J. *et al.* Forest response to elevated CO2 is conserved across a broad range of productivity. *Proc. Natl. Acad. Sci. U. S. A.* **102,** 18052–18056 (2005).

32. Van Groenigen, K. J. *et al.* The Impact of Elevated Atmospheric CO2 on Soil C and N Dynamics. *Ecol. Stud.* **187,** 374–391 (2006).

33. Terrer, C. *et al.* Mycorrhizal association as a primary control of the CO_2 fertilization effect. *Science* **353,** 72–4 (2016).

34. McCarthy, H. R. *et al.* Re-assessment of plant carbon dynamics at the Duke free-air CO2enrichment site: interactions of atmospheric [CO2] with nitrogen and water availability over stand development. *New Phytol.* **185,** 514–528 (2010).

35. Hyvönen, R. *et al.* The likely impact of elevated [CO2], nitrogen deposition, increased temperature and management on carbon sequestration in temperate and boreal forest ecosystems: a literature review. *New Phytol.* **173,** 463–80 (2007).

36. Ryan, M. G. Effects of climate change on plant respiration. *Ecol. Appl.* **1,** 157–167 (1991).

37. Amthor, J. S. Scaling CO2 Photosynthesis Relationships from the Leaf to the

Canopy. *Photosynth. Res.* **39,** 321–350 (1994).

38. Wu, Z., Dijkstra, P., Koch, G. W., Peñuelas, J. & Hungate, B. a. Responses of terrestrial ecosystems to temperature and precipitation change: a meta-analysis of experimental manipulation. *Glob. Chang. Biol.* **17,** 927–942 (2011).

39. Chevallier, F. *et al.* Toward robust and consistent regional CO2 flux estimates from in situ and spaceborne measurements of atmospheric CO2. *Geophys. Res. Lett.* **41,** 1065–1070 (2014).

40. Olivier, J. G. J. & Berdowski, J. J. M. in *The Climate System* (eds. Berdowski, J., Guicherit, R. & Heij, B. J.) 33–78 (2001).

41. Sitch, S. *et al.* Recent trends and drivers of regional sources and sinks of carbon dioxide. *Biogeosciences* **12,** 653–679 (2015).

42. Harris, I., Jones, P. D. D., Osborn, T. J. J. & Lister, D. H. H. Updated high-resolution grids of monthly climatic observations - the CRU TS3.10 Dataset. *Int. J. Climatol.* **34,** online, update (2013).

43. Vicente-serrano, S. M., Beguería, S. & López-Moreno, J. I. A Multiscalar Drought Index Sensitive to Global Warming: The Standardized Precipitation Evapotranspiration Index. *J. Clim.* **23,** 1696–1718 (2010).

44. Zuur, A., Ieno, E., Walker, N., Saveliev, A. & Smith, G. *Mixed effects models and extensions in ecology with R*. (Springer science, 2009).

45. Mathias, J. M. & Thomas, R. B. Disentangling the effects of acidic air pollution, atmospheric CO2, and climate change on recent growth of red spruce trees in the Central Appalachian Mountains. *Glob. Chang. Biol.* **24,** 3938–3953 (2018).

46. R Core Team. R: A Lenguage and Environment for Stasitical Computing. (2016).

47. Barton, K. MuMIn: Multi-model inference. R package version 1.17.1. http://CRAN.R-project.org/package=MuMIn. (2015).

48. Nakagawa, S. & Schielzeth, H. A general and simple method for obtaining R 2 from generalized linear mixed-effects models. *Methods Ecol. Evol.* **4,** 133–142 (2013).

49. Breheny, P. & Burchett, W. Visualization of Regression Models Using visreg, R package version 2.2-0. (2015).

Correspondence and requests for materials should be addressed to:

Marcos Fernández-Martínez: marcos.fernandez-martinez@uantwerpen.be

Acknowledgements

This research was supported by the Spanish Government project CGL2016-79835-P (FERTWARM), the European Research Council Synergy grant ERC-2013-726 SyG-610028 IMBALANCE-P, and the Catalan Government project SGR 2017-1005. M.F-M and S.V. are a postdoctoral fellows of the Research Foundation – Flanders (FWO). J.G.C. thanks the support of the National Environmental Science Programme ESCC Hub. We thank Christian Röedenbeck for his advice and for distributing Jena CarboScope and all the modellers that contributed to the TRENDY project.

Author Contributions

M.F-M., J.S., I.A.J., and J.P. conceived, analyzed and wrote the paper. F.C., P.F., and S.S., provided data. All authors contributed substantially to the writing and discussion of the paper.

Figure captions

Figure 1: Global trends in NEP for the a) MACC-II, b) Jena CarboScope, and c) TRENDY ensemble datasets. Global temporal contributions of CO_2, climate and land-use change to the trends in NEP (annual change) are shown on the right side of each panel. The difference between the modelled temporal contributions and the trends (shaded) has been treated as an unknown contribution to the temporal variation in NEP. Statistically significant ($P < 0.01$) temporal variations of the predictors are shown in square brackets. Error bars indicate 95% confidence intervals. The boxplots in panel c indicate the estimated contributions of the 10 DVGMs used in the TRENDY ensemble. Units are ppm y^{-1} for CO_2, °C y^{-1} for temperature, mm y^{-2} for precipitation, standard deviation for SPEI, and percentage of land-use cover per pixel for forests, crops, and urban areas. See the Materials and Methods section for information about the methodology used to calculate the contributions. Significance levels: *, $P < 0.01$; **, $P < 0.005$; ***, $P < 0.001$.

Figure 2: Plots showing the estimated effects of the interactions of the statistical models. The graphs show interactions between CO_2 and climate (mean annual precipitation [MAP] and temperature [MAT], and annual anomalies in temperature [MAT.an]) on NEP for the MACC-II and Jena CarboScope inversion models and the TRENDY ensemble. Shaded bands indicate the 95% confidence intervals of the slopes. Non-significant interactions are indicated by “n.s.”.

Table 1: Global and latitudinal analyses of sensitivity of NEP to changes in atmospheric CO_2 concentrations and mean annual temperature. The “%” columns indicate the contribution of the latitudinal band to the global estimate. Differences are calculated as the difference between the sum of all latitudinal bands and the global estimate. Bold coefficients differ significantly from 0 at the 0.01 level. Empty cells indicate that anomalies in temperature were not a significant predictor in the models predicting NEP. Units are Tg C y^{-1} ppm^{-1} for CO_2 and Tg C y^{-1} C^{-1} for temperature.

Table 2: Global and latitudinal trends and temporal contributions of changes in atmospheric CO_2 concentrations and mean annual temperature to NEP trends. The “%” columns indicate the percentage of contribution of each latitudinal band to the global estimate. Columns “Cont.” show the percentage of contribution of CO_2 and temperature to the trends in NEP. Column “Other” shows the difference between the NEP trend and the sum of contributions of CO_2 and temperature. If different from zero, it indicates that other factors are contributing to the trends in NEP. The “differences”

rows are calculated as the difference between the sum of all latitudinal bands and the global estimate. NH and SH indicate Northern and Southern Hemispheres, respectively. Bold coefficients differ significantly from 0 at the 0.01 level. Empty cells indicate that anomalies in temperature were not a significant predictor in the models predicting NEP. Units are Tg C y^{-1} for trends, Tg C y^{-1} ppm^{-1} for CO_2 and Tg C y^{-1} C^{-1} for temperature. Errors were calculated using the error propagation method. See the Materials and Methods section for information about the methods used to calculate the contributions.

Figure 1

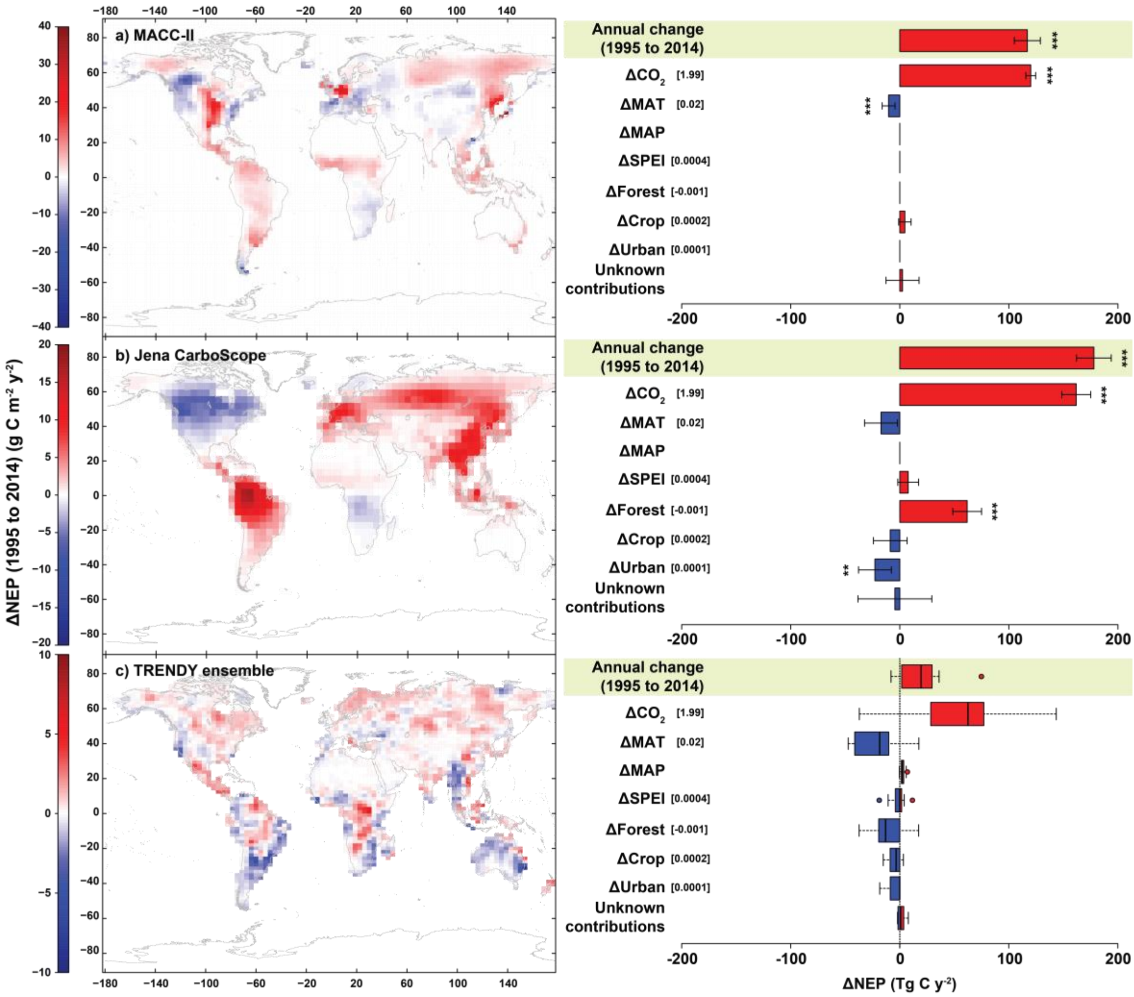

a) MACC-II
b) Jena CarboScope
c) TRENDY ensemble
ΔNEP (1995 to 2014) (g C m-2 y-2)
Annual change (1995 to 2014)
ΔCO2 [1.99]
ΔMAT [0.02]
ΔMAP
ΔSPEI [0.0004]
ΔForest [-0.001]
ΔCrop [0.0002]
ΔUrban [0.0001]
Unknown contributions
ΔNEP (Tg C y-2)

Figure 2

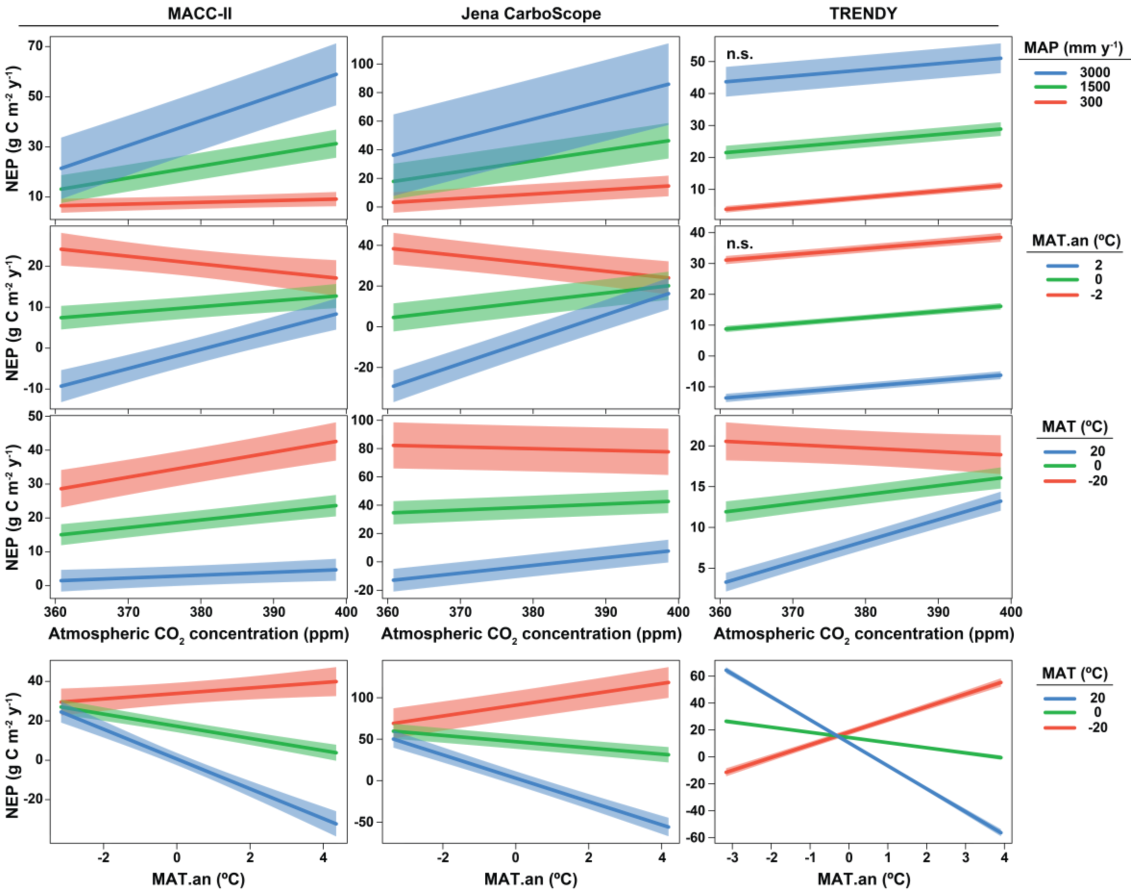
MACC-II
Jena CarboScope
TRENDY
NEP (g C m-2 y-1)
n.s.
MAP (mm y-1)
3000
1500
300
MAT.an (ºC)
2
0
-2
MAT (ºC)
20
0
-20
Atmospheric CO2 concentration (ppm)
MAT.an (ºC)

Table 1

	CO_2	**%**	**Temperature**	**%**
MACC				
NH >55°	**8.5 ± 0.4**	14.1	-35.3 ± 24.1	6.8
NH 35-55°	**14.7 ± 1.3**	24.3	-132.0 ± 259.9	25.6
NH 15-35°	**-5.0 ± 1.4**	-8.3		
NH 15-SH 15°	**31.9 ± 0.7**	52.9	101.9 ± 216.6	-19.8
SH 15-35°	**2.2 ± 0.9**	3.7	-150.2 ± 131.3	29.1
SH 35-55°	0.6 ± 0.3	1.0	-13.4 ± 49.3	2.6
Global	**60.4 ± 1.2**		**-515.7 ± 152.4**	
Difference	**-7.4 ± 2.6**	-12.3	286.6 ± 397.4	-55.6
JENA				
NH >55°	-0.3 ± 1.0	-0.3	-49.8 ± 48.2	5.8
NH 35-55°	**11.1 ± 3.9**	13.6	-213.6 ± 558.1	24.9
NH 15-35°	**26.3 ± 2.7**	32.3	-268.7 ± 400.0	31.3
NH 15-SH 15°	**54.2 ± 3.6**	66.6	-697.6 ± 1136.5	81.2
SH 15-35°	**5.4 ± 0.9**	6.6	-167.0 ± 133.9	19.4
SH 35-55°	**0.2 ± 0.0**	0.3		
Global	**81.4 ± 3.4**		-859.2 ± 386.3	
Difference	15.4 ± 6.9	19.0	-537.4 ± 1390.2	62.5
TRENDY				
NH >55°	**2.8 ± 0.1**	9.0	**17.3 ± 7.3**	-1.6
NH 35-55°	**5.8 ± 0.5**	19.0	**-251.1 ± 79.3**	23.1
NH 15-35°	**5.9 ± 0.6**	19.4	**-368.8 ± 51.9**	33.9
NH 15-SH 15°	**16.6 ± 1.1**	54.2	**-1612.2 ± 213.4**	148.2
SH 15-35°	**4.6 ± 1.2**	14.9	**-379.2 ± 141.1**	34.9
SH 35-55°	0.3 ± 0.2	1.0	-36.8 ± 18.1	3.4
Global	**30.7 ± 1.2**		**-1088.0 ± 118.1**	
Difference	**5.4 ± 2.1**	17.5	**-1542.7 ± 298.0**	141.8

Table 2

	Trends	%	CO_2	%	Cont.	Temp	%	Cont.	Other
MACC									
NH >55°	**20.1 ± 1.2**	17.2	**17.0 ± 0.8**	14.1	84.4	-1.2 ± 0.8	11.5	-5.9	4.3 ± 1.7
NH 35-55°	**17.5 ± 5.0**	15.0	**29.2 ± 2.7**	24.3	166.6	-1.7 ± 3.2	16.1	-9.4	-10.0 ± 6.5
NH 15-35°	**14.0 ± 3.1**	12.0	-9.9 ± 2.8	-8.3	-71.0			0.0	**23.9 ± 4.1**
NH 15-SH 15°	**55.4 ± 2.7**	47.4	**63.5 ± 1.5**	52.9	114.6	0.9 ± 1.9	-8.9	1.6	-9.0 ± 3.6
SH 15-35°	**7.6 ± 1.4**	6.5	**4.4 ± 1.9**	3.7	57.6	-2.3 ± 2.0	22.2	-29.8	5.5 ± 3.1
SH 35-55°	**2.3 ± 0.6**	2.0	1.2 ± 0.7	1.0	49.9	-0.3 ± 1.0	2.5	-11.2	1.4 ± 1.3
Global	**116.9 ± 6.1**		**120.1 ± 2.3**		102.7	**-10.3 ± 3.0**		-8.8	7.1 ± 7.2
Difference	0.0 ± 9.1	0.0	**-14.8 ± 5.2**	-12.3		5.8 ± 5.4	-56.6		
JENA									
NH >55°	**13.8 ± 2.2**	7.7	-0.5 ± 2.1	-0.3	-3.8	-1.7 ± 1.7	9.9	-12.4	**16.0 ± 3.5**
NH 35-55°	**49.8 ± 5.9**	28.0	**22.0 ± 7.7**	13.6	44.1	-2.7 ± 6.9	15.4	-5.3	**30.5 ± 11.9**
NH 15-35°	**49.2 ± 4.0**	27.6	**52.3 ± 5.3**	32.3	106.2	-5.0 ± 7.4	29.0	-10.2	1.9 ± 10.0
NH 15-SH 15°	**80.4 ± 5.1**	45.2	**107.7 ± 7.1**	66.6	133.9	-5.7 ± 9.2	32.9	-7.0	-21.6 ± 12.7
SH 15-35°	**10.4 ± 1.3**	5.8	**10.7 ± 1.7**	6.6	103.1	-2.8 ± 2.2	16.2	-26.9	2.5 ± 3.1
SH 35-55°	**0.5 ± 0.1**	0.3	**0.4 ± 0.1**	0.3	87.2				0.1 ± 0.1
Global	**178.0 ± 8.1**		**161.8 ± 6.8**		90.9	**-17.2 ± 7.7**		-9.7	**33.4 ± 13.1**
Difference	**26.1 ± 12.2**	14.7	**30.7 ± 13.8**	19.0		-0.6 ± 16.0	3.4		
TRENDY									
NH >55°	**9.3 ± 0.6**	41.4	**5.5 ± 0.3**	9.0	59.0	**0.6 ± 0.2**	-2.7	6.1	**3.3 ± 0.7**
NH 35-55°	**9.4 ± 1.3**	41.5	**11.6 ± 0.9**	19.0	124.0	**-3.0 ± 0.9**	13.9	-31.6	0.7 ± 1.8
NH 15-35°	**3.3 ± 1.3**	14.9	**11.8 ± 1.1**	19.4	352.9	**-7.9 ± 1.0**	36.9	-235.0	-0.6 ± 2.0
NH 15-SH 15°	**10.1 ± 2.3**	45.0	**33.0 ± 2.1**	54.2	326.2	**-17.2 ± 1.8**	80.8	-170.2	-5.7 ± 3.6
SH 15-35°	**-13.7 ± 1.8**	-60.9	**0.5 ± 0.1**	0.9	-3.8	**-0.3 ± 0.1**	1.6	2.5	**-13.9 ± 1.8**
SH 35-55°	**-1.0 ± 0.4**	-4.7	**0.6 ± 0.5**	1.0	-55.4	-0.7 ± 0.4	3.5	70.4	-0.9 ± 0.7
Global	**22.5 ± 3.1**		**61.0 ± 2.5**		270.7	**-21.3 ± 2.2**		-94.7	**-17.1 ± 4.5**
Difference	-5.2 ± 4.7	-22.9	2.1 ± 3.6	3.4		**-7.3 ± 3.2**	34.0		

Methods

Datasets

NEP data

We used gridded global monthly NEP data for 1995–2014 from two inversion models: i) the MACC (Monitoring Atmospheric Composition and Climate) CO_2 (http://www.gmes-atmosphere.eu/catalogue/) [25,39] database, version v14r2 and ii) the Jena CarboScope database version s93_v3.7 using a constant network of towers (http://www.bgc-jena.mpg.de/CarboScope/) [26]. The MACC CO_2 atmospheric inversion system relies on the variational formulation of Bayes' theorem to analyse direct measurements of CO_2 concentrations from 130 sites around the globe for 1979-2014. Optimised fluxes were calculated at a global horizontal resolution of 3.75 × 1.875° (longitude, latitude) and a temporal resolution of eight days, separately for daytime and night-time. The underlying transport model was run with interannually varying meteorological data from the ECMWF ERA-Interim reanalysis. The Jena inversion model estimates the interannual variability of CO_2 fluxes based on raw CO_2 concentration data from 50 sites. The model uses a variational approach with the TM3 transport model (4 × 5°, using interannually varying winds). Prior terrestrial fluxes were obtained from a modelled mean biospheric pattern and fossil-fuel emissions from the EDGAR emission database[40]. We also used NEP data from an ensemble of 10 dynamic global vegetation models (DGVMs) compiled by the TRENDY project (version 4, models CLM4.5, ISAM, JSBACH, JULES, LPJG, LPX, OCN, ORCHIDEE, VEGAS, and VISIT) to see if results obtained from atmospheric inversions data match those obtained with DGVMs simulations[41]. We used the output from simulation experiment S3, which was run with varying atmospheric CO_2 and changing land use and climate[41].

Meteorological, land-use change and atmospheric CO_2 data

We extracted gridded temperature and precipitation time series from the Climatic Research Unit TS3.23 dataset [42]. We also used the SPEI (Standardised Precipitation-Evapotranspiration Index) drought index[43] from the global SPEI database (http://SPEI.csic.es/database.html) as a measure of drought intensity (positive values indicate wetter than average meteorological conditions, negative values indicate drier than average conditions). We used annual SPEI1 (monthly SPEI averaged over a year). Mean annual temperature (MAT) and precipitation (MAP) and SPEI were calculated for each year and pixel. We used land-use change maps from land-use harmonisation[2] (LUH2, http://luh.umd.edu/data.shtml) and calculated the percent coverages of forests, croplands, and urban areas per pixel, so we could further estimate whether they increased or decreased from 1995 to 2014. We used the data for atmospheric CO_2 concentration from Mauna Loa Observatory provided by the Scripps Institution of Oceanography (Scripps CO_2 programme).

Data for N and S deposition

Annual data for N (oxidised N [N_{OX}] from NO_3^- and reduced N [N_{RED}] from NH_4^+) and S (SO_4^-) wet deposition were extracted from: i) the European Monitoring and Evaluation Programme (EMEP) with a spatial resolution of 0.15 × 0.15° for longitude and latitude, ii) the MSC-W chemical-transport model developed to estimate regional atmospheric dispersion and deposition of acidifying and eutrophying N and S compounds over Europe, and iii) the National Atmospheric Deposition Program (NADP) covering the USA with a spatial resolution of 0.027 × 0.027° for longitude and latitude. We used only data for wet deposition because the NADP database only contained records for dry deposition for 2000. Analyses focused on atmospheric deposition and were restricted to Europe and the USA because temporal gridded maps of atmospheric deposition were not available for other regions. Maps of atmospheric deposition for the regional analyses were adjusted to the resolution of the C-flux maps (3.75 × 1.875° for the MACC-II model and 4 × 5° for the Jena CarboScope model for longitude and latitude).

Statistical analyses

Gridded, global and regional trend detection on NEP

To determine how NEP has changed from 1995 to 2014, we first calculated the trends for each pixel in both inversion models and an average dataset of the TRENDY ensemble using linear regressions with an autoregressive and moving-average (ARMA) (autoregressive structure at lag p=1, and no moving average q=0) correlation structure to account for temporal autocorrelation. Trends over larger areas (e.g. the entire world, latitudinal bands), either for NEP or the predictor variables, were calculated using generalised linear mixed models (GLMMs) with random slopes, including also random intercepts[44] (e.g. NEP ~ year). We used pixel as the random factor (affecting the intercepts and slopes of the year), and an ARMA (p=1, q=0) correlation structure. All average trends shown were calculated using this methodology.

Calculation of temporal contributions on trends of NEP

The temporal contributions of increasing CO_2, climate (MAT, MAP, and SPEI), and land-use change (forests, croplands, and urban areas) to the observed trends in NEP were assessed for the MACC-II, Jena CarboScope, and TRENDY datasets for the entire world. We repeated the analysis for five latitudinal bands to determine if the contributions of CO_2, climate, and land-use change were globally consistent using MACC-II, Jena CarboScope, and the mean ensemble of the TRENDY datasets. For the MACC-II and Jena CarboScope datasets, we also determined the temporal contribution of atmospheric deposition of N (N_{OX} and N_{RED}) and S to the trends in NEP in a combined analysis that also included CO_2, climatic, and land-use trends. This latter analysis was restricted to Europe and the USA due to the lack of atmospheric-deposition time series for the rest of the world.

The temporal contributions of the predictor variables were calculated following the methodology established in references[5,45], as follows:

i) using a GLMM with an autocorrelation structure for lag 1 (AR1) and using the pixel as the random factor affecting only the intercept, we fitted full models for NEP as a function of CO_2, mean MAT per pixel, annual anomaly of MAT, mean MAP per pixel, annual anomaly of MAP, the annual SPEI, and mean percentage of forested, cropped, and urban areas per pixel and their annual anomalies. We included the first-order interaction terms between CO_2 and all predictors and between the mean values and the anomalies for all predictors (except SPEI, which interacted with mean MAT and MAP). When the interaction term between the means and the anomalies (e.g. MAT mean × MAT anomaly) was included, the model estimated the effect of the anomaly as a function of the average value. This implies a change in the effect of increasing or decreasing the anomalies, depending on the mean for the site (e.g. increasing temperature may have a positive effect in cold climates but a negative effect in warmer climates). For models including atmospheric deposition, we also included the interaction between climatic variables and CO_2 and the interactions between the means and the annual anomalies of atmospheric deposition (N_{OX}, N_{RED}, and S). The models were fitted using maximum likelihood to allow the comparison of models with different fixed factors.

ii) We used the stepwise backwards-forwards model selection (*stepAIC* function in R[46]) from the full models, using the lowest Bayesian information criterion (BIC), to obtain the best model. The amount of the variance explained by the models was assessed using the *r.squaredGLMM* function in R (MuMIn package: [47]) following the method of Nakagawa and Schielzeth (2013). Model residuals met the assumptions required in all analyses (normality and homoscedasticity of residuals).

iii) We then used the selected models to predict the changes of the response variables during the study period (1995–2014). We first extracted the observed trend (mean ± SEM, standard error of the mean) in NEP using raw data with GLMMs with an AR1 autocorrelation structure. We then calculated the trend of NEP predicted by the final model and the trends of NEP predicted by the same model while maintaining the temporally varying predictors (i.e., anomalies) constant one at a time (e.g. MAT anomalies were held constant using the median per pixel, while all other predictors changed based on the observations). The difference between the predictions for the final model and when one predictor was controlled was assumed to be the contribution of that predictor variable to the change in NEP. The differences between all individual contributions and the observed trend in NEP were treated as unknown contributions.

Calculation of sensitivities of NEP to temporal predictors

Finally, we calculated the average sensitivities of NEP to the predictor changes by dividing the temporal contributions of each predictor of delta NEP by their temporal trends. Spatial variability on the effects of temporal predictors to NEP were assessed using the GLMMs fitted to estimate the temporal contributions of the predictors. To visualise the interactions we used the R package visreg [49]. All errors were calculated using the error-propagation method using the following two equations, for additions and subtractions: $\boldsymbol{\varepsilon C} = \sqrt{(\boldsymbol{\varepsilon A})^{\mathbf{2}} + (\boldsymbol{\varepsilon B})^{\mathbf{2}}}$; and for multiplications and divisions: $\boldsymbol{\varepsilon C} = \boldsymbol{C}\sqrt{\left(\frac{\boldsymbol{\varepsilon A}}{\boldsymbol{A}}\right)^{\mathbf{2}} + \left(\frac{\boldsymbol{\varepsilon B}}{\boldsymbol{B}}\right)^{\mathbf{2}}}$; where ε indicates the error associated to each value (A, B or C). To calculate global and regional estimates we multiplied the model outputs, in units of gC m^{-2}, times land area. We considered the land Earth surface area to be 134375000 km^2 excluding the Antarctic region. Land area for the different latitudinal bands used were: >55º N, 23818000 km^2; 35 to 55º N, 31765000 km^2; 15 to 35º N, 29213000 km^2; 15º S to 15º N, 29926000 km^2; 15 to 35º S, 17308000 km^2; and 35 to 55º S, 2345600 km^2.

Supplementary Information

1. Supplementary discussion:

Atmospheric deposition and the terrestrial C balance

The effects of N_{OX} deposition were divergent in both the MACC-II and Jena CarboScope datasets for temporal and spatial variability. Conclusions about the effect of N_{OX} on regional NEP thus cannot be drawn from our analyses. The discrepancy in the results for N_{OX} in **Figure S1** and **Table S1** was due to the different NEP trends for Europe and the USA for both models. N_{RED} did not significantly contribute to the trends in NEP for either of the inversion models (**Figure S1),** mainly because it did not have a significant trend over time. N_{RED}, however, was a significant predictor of spatial and interannual NEP variability (see **Supplementary Information 2.8**), in contrast to N_{OX}. Analysing the deposition of oxidised and reduced N separately rather than only using the total amount of N, as has been done so far[11,14,19,50], may thus lead to a better understanding of the effect of total N deposition because of the different chemical properties of NO_3^- compared to NH_4^+, which is easier to acquire by plants[51]. S deposition did not significantly contribute to the trends in NEP, which contrasts with a recent study using eddy-covariance towers[5]. The lack of an effect of S in this case could be due to the local scale of its effects, which would be lost when analysing larger geographical scales. Also, the fact that this study began some years after S deposition started to decline in both continents (mainly during the 80s[52,53]), may have reduced the potential effect of S. The large spatial heterogeneity of sites in different stages of recovery from S deposition and soil properties, such as soil buffer capacity (pH responses to S inputs), could also play a role obfuscating the effects of S deposition when using data with such a coarse resolution.

References:

50. Janssens, I. a. et al. Reduction of forest soil respiration in response to nitrogen deposition. Nat. Geosci. 3, 315–322 (2010).

51. Xu, G., Fan, X. & Miller, A. J. Plant Nitrogen Assimilation and Use Efficiency. Annu. Rev. Plant Biol. 63, 153–182 (2012).

52. Menz, F. C. & Seip, H. M. Acid rain in Europe and the United States: an update. Environ. Sci. Policy 7, 253–265 (2004).

53. Lajtha, K. & Jones, J. Trends in cation, nitrogen, sulfate and hydrogen ion concentrations in precipitation in the United States and Europe from 1978 to 2010: a new look at an old problem. Biogeochemistry 116, 303–334 (2013).

Figure S1: Temporal contributions of the predictor variables to changes in NEP for the MACC-II and Jena CarboScope datasets. Units are g C m^{-2} y^{-2}. Error bars indicate 95% confidence intervals. Significance levels: *, *P* < 0.01; **, *P* < 0.005; ***, *P* < 0.001.

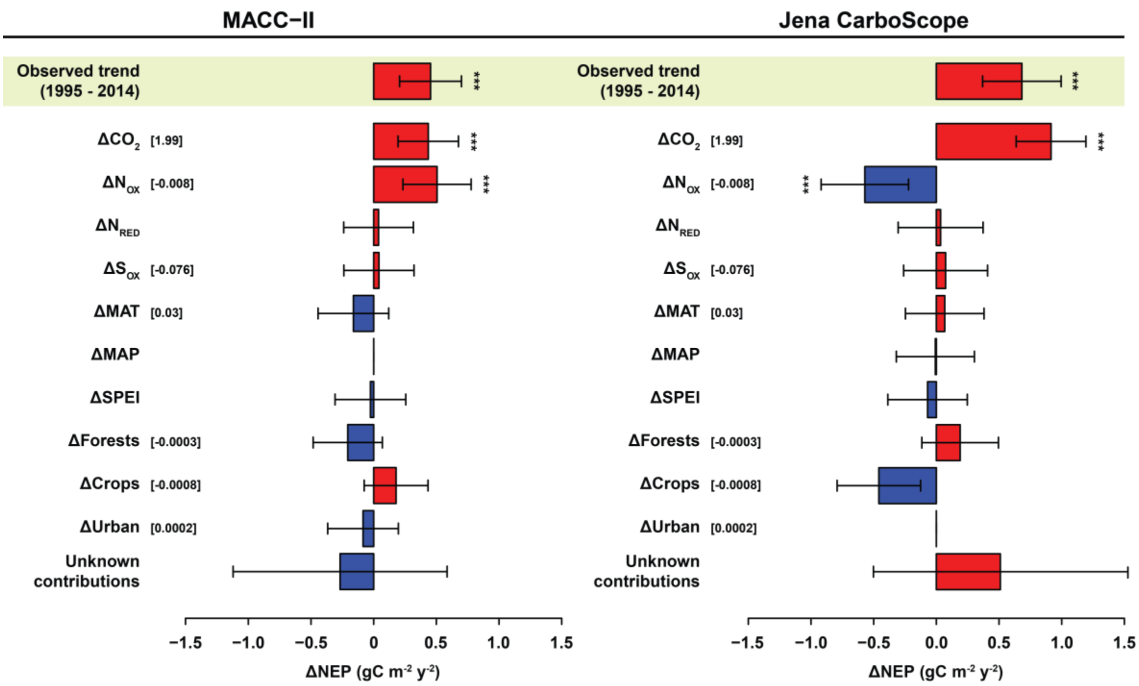

Table S1: Sensitivity of NEP to the predictor variables, including atmospheric deposition for Europe and the USA, for the MACC-II and Jena CarboScope datasets. Units are ppm for CO_2; kg ha^{-1} for N_{OX}, N_{RED}, and S; °C for MAT; mm y^{-1} for MAP, standard deviations for SPEI, and percentage of land-use cover per pixel for forests, crops, and urban areas. Statistically significant estimates are highlighted in bold.

	MACC-II		Jena CarboScope	
	Estimate	***P***	**Estimate**	***P***
CO_2	**0.22 ± 0.06**	**0.0006**	**0.46 ± 0.07**	**<0.0001**
N_{OX}	**-62.32 ± 19.08**	**0.0012**	**49.15 ± 17.12**	**0.0034**
N_{RED}	82.29 ± 357.59	n.s.	-21.60 ± 113.35	n.s.
S	-0.55 ± 1.89	n.s.	-0.84 ± 1.96	n.s.
MAT	-4.75 ± 4.23	n.s.	1.93 ± 4.59	n.s.
MAP	-	-	-0.05 ± 1.04	n.s.
SPEI	-26.58 ± 146.43	n.s.	-55.03 ± 131.25	n.s.
Forests	641.90 ± 440.54	n.s.	-464.58 ± 386.09	n.s.
Crops	-222.48 ± 162.43	n.s.	523.58 ± 203.08	0.0071
Urban	-457.84 ± 772.70	n.s.	-	-

2. Summary of the models predicting interannual variability in NEP (1995–2014)

Abbreviations: cdioxide, atmospheric CO_2 concentration; MAP.c, climatic mean annual precipitation; MAP.an, interannual deviation from the mean in annual precipitation; MAT.c, climatic mean annual temperature; MAT.an, interannual deviation from the mean in annual temperature; SPEI, Standardised Precipitation-Evapotranspiration Index. R^2_m is the variance explained by a fixed factor, and R^2_c is the total variance explained by the model (fixed + random factors). Suffix ".mean" indicates the average value per pixel, while suffix ".an" indicates the temporal anomaly. The two points ":" indicate the interaction between two predictors.

2.1 Global model

MACC-II (R^2_m=0.09; R^2_c=0.49)

	Value	SE	DF	*t*	*P*
(Intercept)	21.281	15.459	54251	1.377	0.1686
cdioxide	-0.055	0.041	54251	-1.357	0.1749
MAP.c	-0.100	0.015	2851	-6.673	<0.0001
MAT.an	-60.487	9.998	54251	-6.050	<0.0001
MAT.c	2.804	0.755	2851	3.716	0.0002
Forests.mean	-107.499	33.336	2851	-3.225	0.0013
Urban.mean	247.026	61.719	54251	4.002	0.0001
Crops.mean	-720.527	67.026	54251	-10.750	<0.0001
Crops.an	4118.938	810.475	54251	5.082	<0.0001
cdioxide:MAP.c	0.000	0.000	54251	8.872	<0.0001
cdioxide:MAT.an	0.152	0.026	54251	5.770	<0.0001
cdioxide:MAT.c	-0.007	0.002	54251	-3.594	0.0003
MAT.an:MAT.c	-0.208	0.026	54251	-8.023	<0.0001
MAP.c:MAT.c	-0.002	0.000	2851	-11.604	<0.0001
cdioxide:Forests.mean	0.340	0.088	54251	3.882	0.0001
cdioxide:Crops.mean	2.096	0.176	54251	11.910	<0.0001
cdioxide:Crops.an	-9.797	2.115	54251	-4.632	<0.0001
Crops.mean:Crops.an	-994.684	152.061	54251	-6.541	<0.0001

Jena CarboScope (R^2_m=0.11; R^2_c=0.82)

	Value	SE	DF	*t*	*P*
(Intercept)	46.927	19.714	21266	2.380	0.0173
cdioxide	-0.093	0.049	21266	-1.879	0.0602
MAP.c	-0.097	0.021	1114	-4.669	<0.0001
MAT.an	-143.210	13.490	21266	-10.616	<0.0001
MAT.c	-7.090	1.057	1114	-6.707	<0.0001
SPEI	-4.637	1.349	21266	-3.437	0.0006
Forests.mean	-16.117	10.138	1114	-1.590	0.1122
Forests.an	235.662	72.477	21266	3.252	0.0011
Urban.an	-1496.360	229.433	21266	-6.522	<0.0001
Crops.mean	-562.384	89.331	1114	-6.296	<0.0001
Crops.an	-454.663	66.259	21266	-6.862	<0.0001
cdioxide:MAP.c	0.000	0.000	21266	7.641	<0.0001
cdioxide:MAT.an	0.369	0.036	21266	10.365	<0.0001
cdioxide:MAT.c	0.017	0.003	21266	6.198	<0.0001
MAT.an:MAT.c	-0.481	0.036	21266	-13.202	<0.0001
MAP.c:MAT.c	-0.002	0.000	1114	-5.703	<0.0001
MAP.c:SPEI	0.006	0.001	21266	5.387	<0.0001
Forests.mean:Forests.an	-1763.944	174.199	21266	-10.126	<0.0001
cdioxide:Crops.mean	1.760	0.230	21266	7.640	<0.0001
Crops.mean:Crops.an	1153.391	204.403	21266	5.643	<0.0001

TRENDY ensemble (R^2_m=0.24; R^2_c=0.46)

	Value	SE	DF	*t*	*P*
(Intercept)	-37.550	6.376	46021	-5.889	<0.0001
cdioxide	0.103	0.017	46021	6.143	<0.0001
MAP.an	0.252	0.027	46021	9.455	<0.0001
MAP.c	0.025	0.001	2418	17.313	<0.0001
MAT.an	-3.818	0.157	46021	-24.248	<0.0001
MAT.c	-2.646	0.306	2418	-8.638	<0.0001
SPEI	-9.012	0.544	46021	-16.554	<0.0001
Forests.mean	-70.832	16.879	2418	-4.197	<0.0001
Forests.an	277.493	24.897	46021	11.146	<0.0001
Urban.an	-378.896	91.627	46021	-4.135	<0.0001
Crops.mean	-1.708	2.346	46021	-0.728	0.4665
Crops.an	-226.309	22.942	46021	-9.865	<0.0001
cdioxide:MAP.an	0.000	0.000	46021	-4.100	<0.0001
MAP.an:MAP.c	0.000	0.000	46021	-58.983	<0.0001
cdioxide:MAT.c	0.008	0.001	46021	9.510	<0.0001
MAT.an:MAT.c	-0.663	0.014	46021	-47.737	<0.0001
MAP.c:MAT.c	-0.001	0.000	2418	-16.146	<0.0001
MAT.c:SPEI	1.104	0.028	46021	39.853	<0.0001
cdioxide:Forests.mean	0.207	0.044	46021	4.666	<0.0001
Forests.mean:Forests.an	-486.559	67.082	46021	-7.253	<0.0001
Crops.mean:Crops.an	296.646	61.259	46021	4.843	<0.0001

2.2 Northern Hemisphere, latitudes >55°

MACC-II (R^2_m=0.22; R^2_c=0.60)

	Value	SE	DF	*t*	*P*
(Intercept)	134.541	26.474	17147	5.082	<0.0001
cdioxide	-0.183	0.068	17147	-2.691	0.0071
MAP.an	-1.714	0.141	17147	-12.205	<0.0001
MAP.c	-0.040	0.007	897	-6.148	<0.0001
MAT.an	-5.546	0.487	17147	-11.379	<0.0001
MAT.c	16.679	1.675	897	9.956	<0.0001
Forests.mean	-231.459	34.121	897	-6.784	<0.0001
Forests.an	7831.834	1975.517	17147	3.964	0.0001
Crops.mean	234.338	29.040	897	8.070	<0.0001
cdioxide:MAP.an	0.005	0.000	17147	12.253	<0.0001
cdioxide:MAT.c	-0.033	0.004	17147	-7.690	<0.0001
MAT.an:MAT.c	-0.439	0.048	17147	-9.219	<0.0001
MAP.c:MAT.c	-0.004	0.001	897	-6.481	<0.0001
cdioxide:Forests.mean	0.627	0.089	17147	7.018	<0.0001
cdioxide:Forests.an	-27.494	5.142	17147	-5.347	<0.0001
Forests.mean:Forests.an	3785.460	356.610	17147	10.615	<0.0001

Jena CarboScope (R^2_m=0.31; R^2_c=0.75)

	Value	SE	DF	*t*	*P*
(Intercept)	-27.173	35.311	6490	-0.770	0.4416
cdioxide	0.279	0.088	6490	3.161	0.0016
MAP.c	-0.035	0.012	336	-3.010	0.0028
MAT.an	-64.639	10.004	6490	-6.461	<0.0001
MAT.c	4.918	0.700	336	7.026	<0.0001
Forests.mean	197.266	59.568	336	3.312	0.001
Forests.an	18735.355	2792.289	6490	6.710	<0.0001
Crops.mean	174.334	42.089	336	4.142	<0.0001
cdioxide:MAT.an	0.164	0.026	6490	6.196	<0.0001
MAT.an:MAT.c	-0.224	0.049	6490	-4.530	<0.0001
MAP.c:MAT.c	-0.005	0.001	336	-3.793	0.0002
cdioxide:Forests.mean	-0.621	0.156	6490	-3.991	0.0001
cdioxide:Forests.an	-58.567	7.282	6490	-8.043	<0.0001
Forests.mean:Forests.an	4383.258	534.136	6490	8.206	<0.0001

TRENDY ensemble (R^2_m=0.29; R^2_c=0.44)

	Value	SE	DF	*t*	*P*
(Intercept)	-66.328	11.678	13040	-5.680	<0.0001
cdioxide	0.247	0.030	13040	8.113	<0.0001
MAP.an	-0.386	0.070	13040	-5.547	<0.0001
MAP.c	-0.001	0.002	681	-0.459	0.6464
MAT.an	20.290	4.335	13040	4.680	<0.0001
MAT.c	-1.307	0.804	681	-1.624	0.1048
SPEI	19.743	2.347	13040	8.411	<0.0001
Forests.mean	41.852	14.892	681	2.810	0.0051
Forests.an	287.470	92.025	13040	3.124	0.0018
Crops.mean	28.292	7.125	681	3.971	0.0001
cdioxide:MAP.an	0.001	0.000	13040	4.669	<0.0001
MAP.an:MAP.c	0.000	0.000	13040	4.239	<0.0001
cdioxide:MAT.an	-0.051	0.011	13040	-4.480	<0.0001
cdioxide:MAT.c	0.009	0.002	13040	4.257	<0.0001
MAP.c:MAT.c	-0.003	0.000	681	-10.990	<0.0001
MAP.c:SPEI	-0.029	0.004	13040	-6.745	<0.0001
MAT.c:SPEI	0.775	0.108	13040	7.205	<0.0001
cdioxide:Forests.mean	-0.123	0.039	13040	-3.152	0.0016
Forests.mean:Forests.an	-812.610	147.719	13040	-5.501	<0.0001

2.3 Northern Hemisphere, latitudes between 35 and 55°

MACC-II (R^2_m=0.13; R^2_c=0.37)

	Value	**SE**	**DF**	***t***	***P***
(Intercept)	148.474	75.069	12204	1.978	0.0480
cdioxide	-0.459	0.197	12204	-2.327	0.0200
MAP.an	0.824	0.174	12204	4.746	<0.0001
MAP.c	-0.388	0.079	638	-4.934	<0.0001
MAT.an	-89.97	24.903	12204	-3.613	0.0003
MAT.c	20.781	6.061	638	3.429	0.0006
Forests.an	-16499.293	4157.812	12204	-3.968	0.0001
Urban.mean	595.477	98.535	12204	6.043	<0.0001
Crops.mean	-869.677	230.863	638	-3.767	0.0002
Crops.an	1277.898	226.561	12204	5.640	<0.0001
cdioxide:MAP.an	-0.002	0.000	12204	-4.842	<0.0001
cdioxide:MAP.c	0.001	0.000	12204	6.182	<0.0001
cdioxide:MAT.an	0.233	0.066	12204	3.556	0.0004
cdioxide:MAT.c	-0.051	0.016	12204	-3.211	0.0013
MAP.c:MAT.c	-0.009	0.001	638	-7.588	<0.0001
cdioxide:Forests.an	44.681	10.947	12204	4.082	<0.0001
cdioxide:Crops.mean	2.664	0.608	12204	4.379	<0.0001
Crops.mean:Crops.an	-3244.474	499.841	12204	-6.491	<0.0001

Jena CarboScope (R^2_m=0.12; R^2_c=0.74)

	Value	SE	DF	*t*	*P*
(Intercept)	-350.099	89.327	4393	-3.919	0.0001
cdioxide	1.220	0.233	4393	5.240	<0.0001
MAP.an	0.032	0.010	4393	3.198	0.0014
MAP.c	-0.291	0.093	226	-3.148	0.0019
MAT.an	-176.873	29.650	4393	-5.965	<0.0001
MAT.c	29.001	7.637	226	3.798	0.0002
SPEI	-24.019	4.322	4393	-5.557	<0.0001
Forests.mean	2909.782	258.050	226	11.276	<0.0001
Forests.an	-2076.464	228.800	4393	-9.075	<0.0001
Urban.mean	787.980	246.180	226	3.201	0.0016
Urban.an	-2473.911	584.642	4393	-4.231	<0.0001
Crops.mean	-1237.354	271.117	226	-4.564	<0.0001
Crops.an	-12046.724	2907.443	4393	-4.143	<0.0001
cdioxide:MAP.c	0.001	0.000	4393	2.946	0.0032
cdioxide:MAT.an	0.466	0.078	4393	5.963	<0.0001
cdioxide:MAT.c	-0.091	0.020	4393	-4.563	<0.0001
MAT.c:SPEI	1.686	0.439	4393	3.843	0.0001
cdioxide:Forests.mean	-7.801	0.675	4393	-11.553	<0.0001
cdioxide:Crops.mean	3.363	0.709	4393	4.746	<0.0001
cdioxide:Crops.an	30.215	7.661	4393	3.944	0.0001
Crops.mean:Crops.an	2766.726	571.8067	4393	4.839	<0.0001

TRENDY ensemble (R^2_m=0.31; R^2_c=0.39)

	Value	SE	DF	*t*	*P*
(Intercept)	-99.108	13.155	11387	-7.534	<0.0001
cdioxide	0.266	0.035	11387	7.702	<0.0001
MAP.an	0.170	0.007	11387	25.662	<0.0001
MAP.c	0.032	0.003	594	12.688	<0.0001
MAT.an	0.222	0.391	11387	0.567	0.5706
MAT.c	4.704	1.230	594	3.823	0.0001
SPEI	20.524	1.903	11387	10.784	<0.0001
Forests.mean	-7.570	2.528	594	-2.995	0.0029
Forests.an	342.651	64.642	11387	5.301	<0.0001
Crops.mean	19.192	2.341	594	8.197	<0.0001
Crops.an	1847.180	590.494	11387	3.128	0.0018
MAP.an:MAP.c	0.000	0.000	11387	-15.519	<0.0001
cdioxide:MAT.c	-0.013	0.003	11387	-3.909	0.0001
MAT.an:MAT.c	-0.672	0.054	11387	-12.362	<0.0001
MAP.c:MAT.c	-0.001	0.000	594	-4.794	<0.0001
MAP.c:SPEI	-0.046	0.003	11387	-14.495	<0.0001
MAT.c:SPEI	1.141	0.132	11387	8.629	<0.0001
Forests.mean:Forests.an	-619.545	135.886	11387	-4.559	<0.0001
cdioxide:Crops.an	-4.959	1.550	11387	-3.199	0.0014

2.4 Northern Hemisphere, latitudes between 15 and 35°

MACC-II (R^2_m=0.10; R^2_c=0.48)

	Value	SE	DF	*t*	*P*
(Intercept)	-79.616	30.449	8352	-2.615	0.0089
cdioxide	0.044	0.071	8352	0.618	0.5369
MAP.an	-0.025	0.010	8352	-2.656	0.0079
MAP.c	-0.069	0.040	435	-1.736	0.0832
MAT.c	2.611	0.590	435	4.428	<0.0001
Forests.mean	2127.100	425.131	435	5.003	<0.0001
Forests.an	434.725	226.387	8352	1.920	0.0549
Crops.an	-710.036	92.556	8352	-7.671	<0.0001
cdioxide:MAP.c	0.000	0.000	8352	5.377	<0.0001
MAP.an:MAP.c	0.000	0.000	8352	3.176	0.0015
MAP.c:MAT.c	-0.006	0.001	435	-7.328	<0.0001
cdioxide:Forests.mean	-5.519	1.1213	8352	-4.922	<0.0001
Forests.mean:Forests.an	-3856.659	779.0509	8352	-4.950	<0.0001

Jena CarboScope (R^2_m=0.40; R^2_c=0.88)

	Value	SE	DF	*t*	*P*
(Intercept)	-43.864	48.290	3395	-0.908	0.3638
cdioxide	0.016	0.082	3395	0.189	0.8498
MAP.an	-0.016	0.004	3395	-4.081	<0.0001
MAP.c	0.145	0.046	173	3.120	0.0021
MAT.an	-171.208	49.580	3395	-3.453	0.0006
MAT.c	1.611	1.526	173	1.055	0.2928
Forests.mean	-2000.599	121.655	173	-16.445	<0.0001
Crops.mean	-561.718	134.866	173	-4.165	<0.0001
cdioxide:MAT.an	0.433	0.131	3395	3.313	0.0009
MAP.c:MAT.c	-0.007	0.002	173	-3.810	0.0002
cdioxide:Forests.mean	6.019	0.305	3395	19.751	<0.0001
cdioxide:Crops.mean	1.794	0.343	3395	5.223	<0.0001

TRENDY ensemble (R^2_m=0.30; R^2_c=0.35)

	Value	SE	DF	*t*	*P*
(Intercept)	-68.340	7.518	7456	-9.090	<0.0001
cdioxide	0.198	0.020	7456	10.124	<0.0001
MAP.an	0.170	0.005	7456	37.363	<0.0001
MAP.c	0.008	0.001	389	12.135	<0.0001
MAT.an	-1.954	1.747	7456	-1.119	0.2633
MAT.c	-0.194	0.061	389	-3.195	0.0015
SPEI	-3.494	1.050	7456	-3.327	0.0009
Forests.mean	-4.296	2.422	389	-1.773	0.0770
Forests.an	-553.870	69.076	7456	-8.018	<0.0001
Crops.an	7186.625	953.175	7456	7.540	<0.0001
MAP.an:MAP.c	0.000	0.000	7456	-30.362	<0.0001
MAT.an:MAT.c	-0.470	0.081	7456	-5.788	<0.0001
MAP.c:SPEI	0.008	0.002	7456	4.898	<0.0001
Forests.mean:Forests.an	1533.238	146.520	7456	10.464	<0.0001
cdioxide:Crops.an	-19.228	2.502	7456	-7.686	<0.0001

2.5 Equatorial belt, latitudes between 15°S and 15°N

MACC-II (R^2_m=0.15; R^2_c=0.48)

	Value	SE	DF	*t*	*P*
(Intercept)	183.608	47.826	9755	3.839	0.0001
cdioxide	0.107	0.081	9755	1.321	0.1867
MAP.an	-0.362	0.062	9755	-5.805	<0.0001
MAP.c	-0.134	0.031	508	-4.390	<0.0001
MAT.an	-673.146	57.219	9755	-11.764	<0.0001
MAT.c	-8.489	1.417	508	-5.993	<0.0001
Forests.mean	-773.117	73.978	508	-10.451	<0.0001
Forests.an	5470.146	1507.142	9755	3.629	0.0003
Crops.mean	-1426.739	189.017	508	-7.548	<0.0001
Crops.an	13000.868	1276.836	9755	10.182	<0.0001
cdioxide:MAP.an	0.001	0.000	9755	5.862	<0.0001
cdioxide:MAT.an	1.727	0.152	9755	11.397	<0.0001
MAP.c:MAT.c	0.005	0.001	508	4.541	<0.0001
cdioxide:Forests.mean	1.833	0.194	9755	9.445	<0.0001
cdioxide:Forests.an	-14.186	3.980	9755	-3.564	0.0004
cdioxide:Crops.mean	3.844	0.497	9755	7.739	<0.0001
cdioxide:Crops.an	-34.276	3.343	9755	-10.255	<0.0001

Jena CarboScope (R^2_m=0.07; R^2_c=0.78)

	Value	SE	DF	*t*	*P*
(Intercept)	-231.111	61.688	4056	-3.746	0.0002
cdioxide	0.576	0.159	4056	3.628	0.0003
MAT.an	-916.973	111.309	4056	-8.238	<0.0001
Forests.mean	-1654.001	183.348	211	-9.021	<0.0001
Forests.an	922.283	165.588	4056	5.570	<0.0001
Urban.an	-3932.951	1345.514	4056	-2.923	0.0035
Crops.mean	-71.310	61.180	211	-1.166	0.2451
Crops.an	9437.141	1957.146	4056	4.822	<0.0001
cdioxide:MAT.an	2.324	0.295	4056	7.875	<0.0001
cdioxide:Forests.mean	4.236	0.478	4056	8.870	<0.0001
Forests.mean:Forests.an	-2347.530	460.780	4056	-5.095	<0.0001
cdioxide:Crops.an	-26.660	5.086	4056	-5.242	<0.0001
Crops.mean:Crops.an	2293.997	497.158	4056	4.614	<0.0001

TRENDY ensemble (R^2_m=0.39; R^2_c=0.60)

	Value	SE	DF	*t*	*P*
(Intercept)	490.827	140.772	8061	3.487	0.0005
cdioxide	-1.569	0.367	8061	-4.278	<0.0001
MAP.an	0.147	0.007	8061	22.211	<0.0001
MAP.c	0.131	0.019	419	7.042	<0.0001
MAT.an	10.027	9.465	8061	1.059	0.2895
MAT.c	-26.543	5.550	419	-4.783	<0.0001
SPEI	64.166	12.534	8061	5.120	<0.0001
Forests.mean	29.681	5.594	419	5.306	<0.0001
Forests.an	4054.263	916.317	8061	4.425	<0.0001
Urban.an	-1831.333	493.907	8061	-3.708	0.0002
Crops.mean	-106.331	9.997	419	-10.636	<0.0001
Crops.an	-167.024	26.050	8061	-6.412	<0.0001
MAP.an:MAP.c	0.000	0.000	8061	-20.128	<0.0001
cdioxide:MAT.c	0.083	0.015	8061	5.743	<0.0001
MAT.an:MAT.c	-2.361	0.374	8061	-6.308	<0.0001
MAP.c:MAT.c	-0.005	0.001	419	-7.071	<0.0001
MAP.c:SPEI	0.009	0.003	8061	3.482	0.0005
MAT.c:SPEI	-2.052	0.494	8061	-4.151	<0.0001
cdioxide:Forests.an	-10.149	2.418	8061	-4.197	<0.0001
Forests.mean:Forests.an	-610.824	134.759	8061	-4.533	<0.0001

2.6 Southern Hemisphere, latitudes between 15 and 35°

MACC-II (R^2_m=0.09; R^2_c=0.58)

	Value	SE	DF	*t*	*P*
(Intercept)	-242.440	82.133	5081	-2.952	0.0032
cdioxide	0.660	0.212	5081	3.126	0.0018
MAP.an	0.380	0.097	5081	3.907	0.0001
MAP.c	-0.100	0.031	262	-3.280	0.0012
MAT.an	-4.550	1.104	5081	-4.116	<0.0001
MAT.c	11.390	3.814	262	2.986	0.0031
Forests.mean	-572.320	192.578	262	-2.972	0.0032
Forests.an	-825.520	86.080	5081	-9.590	<0.0001
Urban.mean	735.440	315.200	262	2.333	0.0204
Urban.an	-4607.060	680.517	5081	-6.770	<0.0001
Crops.an	284.940	40.948	5081	6.958	<0.0001
cdioxide:MAP.an	0.000	0.000	5081	-3.806	0.0001
cdioxide:MAT.c	-0.030	0.010	5081	-3.038	0.0024
MAP.c:MAT.c	0.000	0.001	262	3.389	0.0008
cdioxide:Forests.mean	1.530	0.504	5081	3.026	0.0025
Forests.mean:Forests.an	2305.430	391.332	5081	5.891	<0.0001
Urban.mean:Urban.an	81024.440	14792.053	5081	5.478	<0.0001

Jena CarboScope (R^2_m=0.15; R^2_c=0.95)

	Value	SE	DF	*t*	*P*
(Intercept)	-19.308	19.218	2066	-1.005	0.3152
cdioxide	0.063	0.042	2066	1.502	0.1332
MAT.an	-183.420	32.543	2066	-5.636	<0.0001
Forests.mean	-1077.137	124.092	106	-8.680	<0.0001
Crops.mean	-384.891	89.924	106	-4.280	<0.0001
Crops.an	213.558	34.207	2066	6.243	<0.0001
cdioxide:MAT.an	0.457	0.086	2066	5.336	<0.0001
cdioxide:Forests.mean	2.798	0.283	2066	9.882	<0.0001

TRENDY ensemble (R^2_m=0.55; R^2_c=0.60)

	Value	**SE**	**DF**	***t***	***P***
(Intercept)	-45.408	17.113	4816	-2.653	0.0080
cdioxide	0.174	0.043	4816	4.088	<0.0001
MAP.an	0.346	0.009	4816	39.371	<0.0001
MAP.c	-0.041	0.011	248	-3.612	0.0004
MAT.an	-22.058	0.997	4816	-22.129	<0.0001
MAT.c	-0.640	0.289	248	-2.211	0.0280
SPEI	-23.135	3.024	4816	-7.651	<0.0001
Forests.mean	-649.653	162.990	248	-3.986	0.0001
Forests.an	-7245.744	1048.986	4816	-6.907	<0.0001
Urban.an	-1210.500	308.180	4816	-3.928	0.0001
Crops.mean	-38.742	10.446	248	-3.709	0.0003
MAP.an:MAP.c	0.000	0.000	4816	-28.136	<0.0001
MAP.c:MAT.c	0.002	0.001	248	3.365	0.0009
MAP.c:SPEI	0.043	0.004	4816	10.075	<0.0001
cdioxide:Forests.mean	1.755	0.429	4816	4.089	<0.0001
cdioxide:Forests.an	20.440	2.740	4816	7.460	<0.0001

2.7 Southern Hemisphere, latitudes between 35 and 55°

MACC-II (R^2_m=0.16; R^2_c=0.29)

	Value	SE	DF	*t*	*P*
(Intercept)	841.089	175.678	1664	4.788	<0.0001
cdioxide	-2.235	0.463	1664	-4.828	<0.0001
MAT.an	20.909	7.317	1664	2.858	0.0043
MAT.c	-67.293	15.352	84	-4.383	<0.0001
Forests.mean	118.721	23.271	84	5.102	<0.0001
Forests.an	-12027.914	2731.858	1664	-4.403	<0.0001
Crops.mean	-1729.768	445.845	84	-3.880	0.0002
Crops.an	267.144	68.516	1664	3.899	0.0001
cdioxide:MAT.c	0.181	0.041	1664	4.472	<0.0001
MAT.an:MAT.c	-2.178	0.630	1664	-3.455	0.0006
cdioxide:Forests.an	30.931	7.120	1664	4.344	<0.0001
cdioxide:Crops.mean	4.530	1.175	1664	3.855	0.0001

Jena CarboScope (R^2_m=0.003; R^2_c=0.95)

	Value	SE	DF	*t*	*P*
(Intercept)	-39.683	8.216	834	-4.830	<0.0001
cdioxide	0.097	0.019	834	5.180	<0.0001
Crops.an	68.632	11.319	834	6.063	<0.0001

TRENDY ensemble (R^2_m=0.46; R^2_c=0.58)

	Value	SE	DF	*t*	*P*
(Intercept)	350.908	67.256	1206	5.218	<0.0001
cdioxide	-0.925	0.177	1206	-5.243	<0.0001
MAP.an	0.037	0.012	1206	2.955	0.0032
MAP.c	0.012	0.002	60	5.191	<0.0001
MAT.an	37.053	5.352	1206	6.924	<0.0001
MAT.c	-31.635	5.807	60	-5.448	<0.0001
SPEI	-18.042	7.769	1206	-2.322	0.0204
Crops.mean	-35.806	12.237	60	-2.926	0.0048
Crops.an	-7670.795	829.101	1206	-9.252	<0.0001
cdioxide:MAT.c	0.084	0.015	1206	5.483	<0.0001
MAT.an:MAT.c	-3.921	0.450	1206	-8.712	<0.0001
MAP.c:SPEI	-0.042	0.006	1206	-7.507	<0.0001
MAT.c:SPEI	6.182	0.592	1206	10.445	<0.0001
cdioxide:Crops.an	19.649	2.153	1206	9.126	<0.0001

2.8 Europe and the USA (analyses of atmospheric deposition)

Additional abbreviations: N_{OX}.mean, oxidised nitrogen deposition averaged per pixel; N_{OX}.an, N_{OX} interannual deviation from the mean; N_{RED}.mean, reduced nitrogen deposition averaged per pixel; N_{RED}.an, N_{RED} interannual deviation from the mean; S.mean, mean S deposition per pixel; and S.an, S interannual deviation from the mean.

MACC-II (R^2_m=0.22; R^2_c=0.49)

	Value	SE	DF	*t*	*P*
(Intercept)	-40.893	35.980	12635	-1.137	0.2558
cdioxide	0.044	0.094	12635	0.468	0.6396
N_{OX}.mean	33.048	6.284	656	5.259	<0.0001
N_{OX}.an	481.225	82.496	12635	5.833	<0.0001
N_{RED}.mean	-299.383	28.774	656	-10.405	<0.0001
N_{RED}.an	15.835	2.507	12635	6.316	<0.0001
S.mean	183.977	15.764	656	11.671	<0.0001
S.an	-0.005	1.149	12635	-0.004	0.9965
MAP.c	-0.008	0.008	656	-0.980	0.3274
MAT.an	-118.061	22.241	12635	-5.308	<0.0001
MAT.c	0.396	0.255	656	1.551	0.1214
SPEI	-7.308	1.844	12635	-3.963	0.0001
Forests.mean	55.145	9.435	656	5.845	<0.0001
Forests.an	-16349.819	4977.417	12635	-3.285	0.001
Urban.mean	299.800	90.998	12635	3.295	0.001
Urban.an	476.701	612.090	12635	0.779	0.4361
Crops.mean	-3.279	16.432	656	-0.200	0.8419
Crops.an	1094.763	159.344	12635	6.870	<0.0001
cdioxide:N_{OX}.an	-1.329	0.220	12635	-6.037	<0.0001
cdioxide:N_{RED}.mean	0.836	0.075	12635	11.114	<0.0001
cdioxide:S.mean	-0.440	0.041	12635	-10.710	<0.0001
N_{OX}.an:S.an	4.108	1.204	12635	3.412	0.0006
N_{OX}.mean:S.mean	-7.487	0.887	656	-8.444	<0.0001
cdioxide:MAT.an	0.297	0.059	12635	5.066	<0.0001
MAP.c:MAT.c	-0.005	0.000	656	-9.135	<0.0001
cdioxide:Forests.an	49.106	13.067	12635	3.758	0.0002
Forests.mean:Forests.an	-4423.097	705.891	12635	-6.266	<0.0001
Urban.mean:Urban.an	-17270.851	5511.130	12635	-3.134	0.0017
Crops.mean:Crops.an	-3545.647	350.347	12635	-10.120	<0.0001

Jena CarboScope (R^2_m=0.33; R^2_c=0.73)

	Value	SE	DF	*t*	*P*
(Intercept)	94.055	57.772	4539	1.628	0.1036
cdioxide	-0.088	0.149	4539	-0.592	0.5536
N_{OX}.mean	36.936	11.080	232	3.334	0.0010
N_{OX}.an	-824.383	139.292	4539	-5.918	<0.0001
N_{RED}.mean	-321.085	31.616	232	-10.156	<0.0001
N_{RED}.an	403.022	119.088	4539	3.384	0.0007
S.mean	-16.923	3.351	232	-5.050	<0.0001
S.an	250.057	45.066	4539	5.549	<0.0001
MAP.an	0.068	0.015	4539	4.688	<0.0001
MAP.c	0.227	0.080	232	2.850	0.0048
MAT.an	-97.148	28.983	4539	-3.352	0.0008
MAT.c	-1.785	0.601	232	-2.970	0.0033
SPEI	0.618	4.212	4539	0.147	0.8833
Forests.mean	-25.323	24.202	232	-1.046	0.2965
Forests.an	27919.339	5827.135	4539	4.791	<0.0001
Crops.mean	-94.767	31.392	232	-3.019	0.0028
Crops.an	516.327	84.094	4539	6.140	<0.0001
cdioxide:N_{OX}.an	2.206	0.373	4539	5.911	<0.0001
cdioxide:N_{RED}.mean	0.924	0.081	4539	11.430	<0.0001
cdioxide:N_{RED}.an	-1.131	0.313	4539	-3.607	0.0003
N_{RED}.mean:N_{RED}.an	5.735	1.741	4539	3.295	0.001
cdioxide:S.an	-0.659	0.121	4539	-5.457	<0.0001
N_{OX}.an:N_{RED}.an	49.57	6.295	4539	7.875	<0.0001
N_{RED}.an:S.an	-13.216	3.089	4539	-4.279	<0.0001
cdioxide:MAP.c	-0.001	0.000	4539	-3.456	0.0006
cdioxide:MAT.an	0.26	0.076	4539	3.403	0.0007
MAP.c:SPEI	-0.027	0.009	4539	-3.107	0.0019
cdioxide:Forests.an	-77.124	15.423	4539	-5.000	<0.0001
Forests.mean:Forests.an	2464.264	776.224	4539	3.175	0.0015